Robotica (2011) volume 29, pp. 853–862. © Cambridge University Press 2011
doi:10.1017/S0263574711000063

A symmetric parallel Schönflies-motion manipulator for pick-and-place operations

O. Altuzarra, B. Şandru, Ch. Pinto and V. Petuya*

Mechanical Engineering Department, University of the Basque Country UPV/EHU, Alameda de Urquijo s/n 48013 Bilbao, Spain

(Received in Final Form: January 17, 2011. First published online: February 25, 2011)

SUMMARY

This paper presents a new symmetric parallel Schönflies-motion generator. The design is an evolution of a previous robot with linear inputs. The complete kinematic analysis of the 4-degree-of-freedom (dof) parallel manipulator is presented. The degrees of freedom are obtained from the Group Theory, the direct and inverse position problems are solved obtaining the manipulator's workspace, and the Jacobian analysis is presented. Then the isotropic configurations of the manipulator are discussed and the local dexterity map within the workspace is produced. Finally, two alternatives of a rotational mechanical device, which will increase the angular end-effector range, are proposed.

KEYWORDS: Lower-mobility parallel manipulator; Groups of displacements; Kinematic analysis; Workspace; Dexterity.

1. Introduction

Parallel manipulators are complex mechanical systems composed of a moving platform (MP) connected to a base platform by at least two kinematic chains, called limbs. The best known 6-degrees-of-freedom (dof) parallel manipulator is the Gough–Stewart platform, which was introduced for the first time by Gough in the early 1950s and by Stewart in 1965 as a flight simulator. However, these 6-dof parallel manipulators have some major drawbacks, such as a limited workspace and a large number of direct kinematic problem solutions.

Recently an increasing number of researchers have been involved in the study of parallel manipulators with fewer than 6-dof, especially with 3- and 4-dof manipulators. Moreover, in many industrial applications where operations, such as pick-and-place, are essential, 3- or 4-dof parallel manipulators are easier to implement. The Delta robot is a typical example of such manipulators. These manipulators are often called low-mobility parallel manipulators.[1] Some of the advantages of this type of manipulator are a simpler forward position analysis or a larger workspace. A significant amount of research has been focused on the study of parallel manipulators with fewer than 6-dof as shown in ref. [2–4]. A wide overview of low-mobility parallel architecture is also presented in ref. [5].

For most pick-and-place operations, low-mobility parallel manipulators are preferable. In fact, the ones which best correspond with this type of operation are those whose displacements involving the four-dimensional Schönflies subgroup,[6] i.e., three translations and one rotation about a normal axis to the moving platform. This kind of motion is also termed as 3T1R motion or SCARA[1] motion. However, the SCARA systems are often related to the 4-dof serial manipulators, meanwhile the Schönflies-motion generators have a more general character based on the Group Theory developed in ref. [7]. Thus, the Schönflies subgroup is in generally related to parallel architectures.

Since the turn of the century, various parallel robot architectures with low-mobility Schönflies generators have been presented. In ref. [8], an extensive list of this kind of manipulators is given. Angeles *et al.*[9] proposed a 4-dof parallel manipulator with only two limbs, designed with the purpose of achieving high speeds and a large workspace. The kinetostatic conditioning of general two-limbs Schönflies-motion generators is also presented by Gauthier *et al.*,[10] whereas Richard *et al.*[11] proposed a partially decoupled Schönflies-motion generator. However, many of the cited manipulators lack symmetry in their topological design. The H4 parallel robot that Company *et al.*[12] have described is also a typical example of low-mobility Schönflies-motion generator. The end-effector is controlled by an articulated traveling plate, which is composed by two main parts linked together in such way that the traveling plate forms a Π-joint. This produces a rotational motion at the links between parts of the traveling plate on the normal axis. As an alternative, Salgado *et al.*[13] proposed a family of manipulators that are symmetrical, i.e., the four limbs are identical, the number of limbs is equal to the number of degrees of freedom of the moving platform, the type and number of joints in all the limbs are grouped in an identical pattern, and the number and location of actuated joints in all the limbs are the same.[14] The parallel robot presented by the authors in that paper has linear actuators and it is shown in Fig. 1.

In this paper we have undertaken a complete kinematic analysis of a low-mobility parallel manipulator with Schönflies motion. The motion pattern is defined by three translational degrees of freedom and one rotational degree of freedom about an axis normal to the moving platform. The design overcomes the drawbacks of the one developed

* Corresponding author. E-mail: victor.petuya@ehu.es

[1] Selective-Compliance Assembly Robot Arm.

https://doi.org/10.1017/S0263574711000063 Published online by Cambridge University Press



Fig. 1. Symmetric Schönflies-motion generator with linear inputs.

in ref. [13]. This means that the manipulator presented here not only reaches higher velocities and accelerations of the moving platform but also has a larger workspace volume. The kinematic chains of this manipulator are connected with a fixed base platform at one end and a moving platform at the other. Unlike other designs, such as that presented in ref. [12], the moving platform is a unique rigid element. As a result of this, the manipulator provides a higher rigidity and a simpler manufacturing solution than other designs.

First, the degrees of freedom of the manipulator are obtained using the Group Theory. The classification of the kinematic chain subgroups is described, and the manipulator is associated with a corresponding subgroup. Next, the kinematic analysis is completed, solving the inverse and direct problems. The workspace volume is also geometrically computed as the intersection of four tori as a function of the design parameters. Then, differentiating the position equations, the Jacobian analysis is carried out. The singularity locus is found and the dexterity analysis within the workspace is computed numerically. Then two design alternatives are presented for a rotational mechanical device in order to amplify the angular range up to $\pm 180^\circ$. Finally, some conclusions are presented.

2. Degrees of Freedom and Displacement Group

The degree of freedom of the Schönflies-motion generator presented in the paper is easily derived using the Group Theory.

The robot under study is supplied with four identical limbs of the $RR\Pi RR$ type and has a symmetry plane π at $x = -y$, as shown in Fig. 2(a). Each limb has five joints: R is the actuated revolute joint of axis of rotation $\mathcal{A}_i$ and passing through A_i parallel either to $\mathbf{j}$ for $i = 1, 3$ or to $\mathbf{i}$ for $i = 2, 4$, where $\{\mathbf{i}, \mathbf{j}, \mathbf{k}\}$ form an orthonormal triplet fixed to the base platform; R is of axis $\mathcal{B}_i$ parallel to A_i, as shown in Fig. 2(b), and passing through B_i; Π is a parallelogram joint of plane of normal $\mathbf{n}_i$ and allowing for relative translations around circles of radius $\overline{B_iC_i}$; R of axis $\mathcal{C}_i$ parallel to $\mathcal{B}_i$ and passing through C_i; and R of axis $\mathcal{D}_i$ passing through D_i and parallel to $\mathbf{k}$.

The bond $\mathcal{L}_i$ of the ith limb is the product of five bonds, which are as follows:

(i) The rotation subgroup $\mathcal{R}(\mathcal{A}_i)$ axis of rotation $\mathcal{A}_i$ passing through A_i parallel either to $\mathbf{j}$ for $i = 1, 3$ or $\mathbf{i}$ for $i = 2, 4$.
(ii) The rotation subgroup $\mathcal{R}(\mathcal{B}_i)$ of axis of rotation $\mathcal{B}_i$ passing through B_i and parallel to $\mathcal{A}_i$.
(iii) The set of displacements $\mathcal{D}_\Pi(\mathbf{n}_i)$ associated with the Π-joint, characterized by translations around circles of radius $\overline{B_iC_i}$ lying in a plane normal to $\mathbf{n}_i$.
(iv) The rotation subgroup $\mathcal{R}(\mathcal{C}_i)$ of axis of rotation $\mathcal{C}_i$ passing through C_i and parallel to $\mathcal{B}_i$.
(v) The rotation subgroup $\mathcal{R}(\mathcal{D}_i)$ of axis of rotation $\mathcal{D}_i$ passing through D_i and parallel to $\mathbf{k}$.

Hence, the product of the first four bonds is the Schönflies group. For limbs 1 and 3

$$\mathcal{X}(\mathbf{j}) = \mathcal{R}(\mathcal{A}_i) \cdot \mathcal{R}(\mathcal{B}_i) \cdot \mathcal{D}_\Pi(\mathbf{n}_i) \cdot \mathcal{R}(\mathcal{C}_i), \quad i = 1,\ 3, \tag{1}$$

and for limbs 2 and 4

$$\mathcal{X}(\mathbf{i}) = \mathcal{R}(\mathcal{A}_i) \cdot \mathcal{R}(\mathcal{B}_i) \cdot \mathcal{D}_\Pi(\mathbf{n}_i) \cdot \mathcal{R}(\mathcal{C}_i), \quad i = 2,\ 4. \tag{2}$$

Then the kinematic bonds are

$$\mathcal{L}_i = \mathcal{X}(\mathbf{j}) \cdot \mathcal{R}(\mathcal{D}_i), \quad i = 1,\ 3, \tag{3}$$

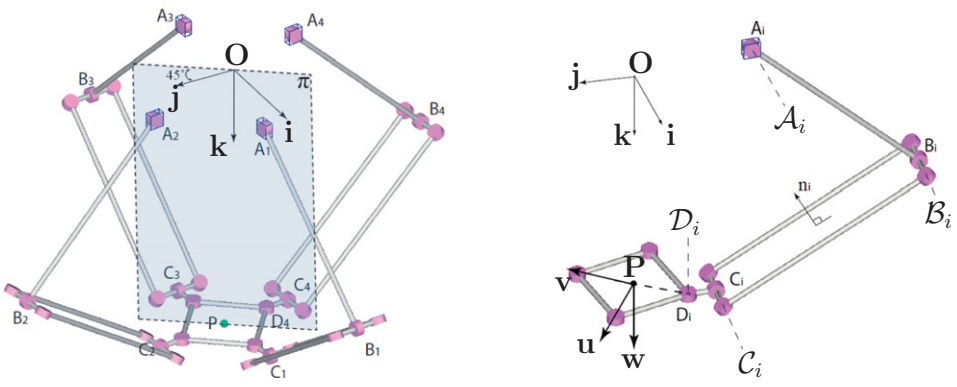


Fig. 2. Symmetric Schönflies-motion generator with rotational inputs.

https://doi.org/10.1017/S0263574711000063 Published online by Cambridge University Press

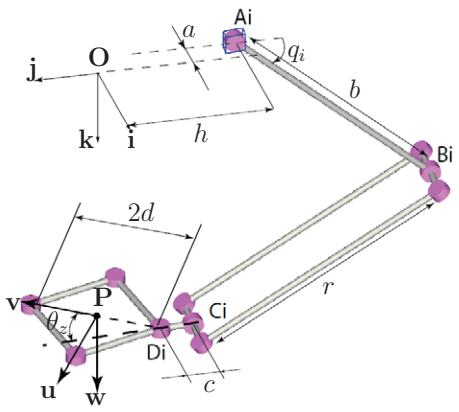


Fig. 3. Design parameters of the manipulator.

and

$$\mathcal{L}_i = \mathcal{X}(\mathbf{i}) \cdot \mathcal{R}(\mathcal{D}_i), \quad i = 2,\ 4. \tag{4}$$

However, notice that the following applies:

$$\mathcal{X}(\mathbf{i}) \cdot \mathcal{R}(\mathcal{D}_i) \equiv \mathcal{X}(\mathbf{k}) \cdot \mathcal{R}(\mathcal{C}_i), \quad i = 1,\ 3, \tag{5}$$

$$\mathcal{X}(\mathbf{j}) \cdot \mathcal{R}(\mathcal{D}_i) \equiv \mathcal{X}(\mathbf{k}) \cdot \mathcal{R}(\mathcal{C}_i), \quad i = 2,\ 4, \tag{6}$$

whence,

$$\mathcal{L}_i = \mathcal{X}(\mathbf{k}) \cdot \mathcal{R}(\mathcal{C}_i), \quad i = 1, \ldots, 4. \tag{7}$$

Therefore, the intersection of the four limbs yields

$$\mathcal{L}_j \cap \mathcal{L}_i = \mathcal{X}(\mathbf{k}) \quad j,\ i = 1, \ldots, 4; \quad j \neq i, \tag{8}$$

thereby proving that, indeed, the intersection of all subsets of limb displacements is a subgroup of $\mathcal{D}$, namely, the Schönflies subgroup $\mathcal{X}(\mathbf{k})$ whose dimension, and hence degrees of freedom, is 4.

3. Kinematics Modeling

As shown in Fig. 2(b), the position of the operation point (OP) P can be expressed for limb i as

$$\mathbf{p} = \mathbf{a}_i + (\mathbf{b}_i - \mathbf{a}_i) + (\mathbf{c}_i - \mathbf{b}_i) + (\mathbf{d}_i - \mathbf{c}_i) + (\mathbf{p} - \mathbf{d}_i),$$
$$i = 1, \ldots, 4, \tag{9}$$

where the position vector of a given point X_i is denoted by the corresponding subscripted lower case boldface vector, $\mathbf{x}_i$. Moreover, the position vectors of points A_i, located in the same plane, are given as

$$\begin{aligned} \mathbf{a}_1 &= -\mathbf{a}_3 = h\mathbf{i} + a\mathbf{j}, \\ \mathbf{a}_2 &= -\mathbf{a}_4 = a\mathbf{i} + h\mathbf{j}, \end{aligned} \tag{10}$$

where h and a are the distances from the fixed frame origin as shown in Fig. 3. By virtue of the given architecture, vectors $\mathbf{b}_i - \mathbf{a}_i$ are expressed in terms of the actuated-joint variables q_i and the length b of limbs $\overline{A_i B_i}$, namely,

$$\mathbf{b}_i - \mathbf{a}_i = b\,(k\mathbf{i}\cos q_1 + \mathbf{k}\sin q_1)\,, \ i = 1, \ldots, 4, \tag{11}$$

and

$$k = \begin{cases} 1, & i = 1, 2, \\ -1, & i = 3, 4. \end{cases} \tag{12}$$

Further, vectors $\mathbf{d}_i - \mathbf{c}_i$ are given as

$$\mathbf{d}_i - \mathbf{c}_i = -kc\,\mathbf{i}, \ i = 1, \ldots, 4, \tag{13}$$

where c is the distance $\overline{C_i D_i}$.

By virtue of the given architecture, links $C_i D_i$ are constrained to move under spatial translations, which explains why these are constant.

Vectors $\mathbf{p}_i - \mathbf{d}_i$, expressed in a local frame $\mathcal{M}$ (**Puvw**) attached to the moving platform, are placed on the four vertices of a square of semi-diagonal d as shown in Fig. 3, namely,

$$\mathbf{p}_i - \mathbf{d}_i = kd\,\mathbf{u}, \ i = 1, \ldots, 4, \tag{14}$$

where $\{\mathbf{u}, \mathbf{v}, \mathbf{w}\}$ is an orthonormal triplet of vectors moving with the moving platform.

The transformation of the vector triplets is given by

$$\begin{aligned} \mathbf{u} &= \mathbf{i}\,\cos\theta_z + \mathbf{j}\,\sin\theta_z, \\ \mathbf{v} &= -\mathbf{i}\,\sin\theta_z + \mathbf{j}\,\cos\theta_z, \\ \mathbf{w} &= \mathbf{k}, \end{aligned} \tag{15}$$

where θ_z being the angle of orientation of the moving platform with respect to the base platform.

Whence the matrix $\mathbf{R}$ that rotates frame $\mathcal{M}$ into $\mathcal{B}$ is derived as

$$\mathbf{R} = \begin{bmatrix} \cos\theta_z & -\sin\theta_z & 0 \\ \sin\theta_z & \cos\theta_z & 0 \\ 0 & 0 & 1 \end{bmatrix}. \tag{16}$$

As vectors $\mathbf{c}_i - \mathbf{b}_i$ must satisfy the constraints imposed by rigid links $B_i C_i$,

$$\|\mathbf{c}_i - \mathbf{b}_i\|^2 = r^2 \quad i = 1, \ldots, 4, \tag{17}$$

with r denoting the common length $\overline{B_i C_i}$, for $i = 1, \ldots, 4$, the resultant system of nonlinear equations is used to solve the position problems:

$$(x + d\cos\theta_z + c - h - b\cos q_1)^2 + (y + d\sin\theta_z - a)^2 + (z - b\sin q_1)^2 = r^2, \tag{18}$$

$$(x - d\sin\theta_z - a)^2 + (y + d\cos\theta_z + c - h - b\cos q_2)^2 + (z - b\sin q_2)^2 = r^2, \tag{19}$$

$$(x - d\cos\theta_z - c + h + b\cos q_3)^2 + (y - d\sin\theta_z + a)^2 + (z - b\sin q_3)^2 = r^2, \tag{20}$$

$$(x + d\sin\theta_z + a)^2 + (y - d\cos\theta_z - c + h + b\cos q_4)^2 + (z - b\sin q_4)^2 = r^2. \tag{21}$$

https://doi.org/10.1017/S0263574711000063 Published online by Cambridge University Press

3.1. Direct position problem

In the direct position problem q_i, input values are known and the solution provides the corresponding x, y, z and θ_z values. In order to solve this problem, the aim is to obtain an univariate polynomial. Equations (18)–(21) define four spheres whose common intersection point provides the end-effector's possible positions, their centers lie at points $C_i(c_{ix}, c_{iy}, c_{iz})$:

$$C_1 : (-d\cos\theta_z - c + h + b\cos q_1, -d\sin\theta_z + a, b\sin q_1), \tag{22}$$

$$C_2 : (d\sin\theta_z + a, -d\cos\theta - c + h + b\cos q_2, b\sin q_2), \tag{23}$$

$$C_3 : (d\cos\theta_z + c - h - b\cos q_3, d\sin\theta_z - a, b\sin q_3), \tag{24}$$

$$C_4 : (-d\sin\theta_z - a, +d\cos\theta_z + c - h - b\cos q_4, b\sin q_4). \tag{25}$$

Operating with Eqs. (18)–(21) and making the following operations $(18) - (19) - (20) + (21)$, $(18) + (19) - (20) - (21)$, and $(18) - (19) + (20) - (21)$, a system of three linear equations is obtained:

$$\begin{aligned} Q_1 x + G_1 y + T_1 z + R_1 &= 0, \\ Q_2 x + G_2 y + T_2 z + R_2 &= 0, \\ Q_3 x + G_3 y + T_3 z + R_3 &= 0, \end{aligned} \tag{26}$$

where the following coefficients depend on θ_z:

$$\begin{aligned} Q_1 =& -2c_{1x} + 2c_{3x} - 2c_{4x} + 2c_{2x}, \\ Q_2 =& -2c_{1x} + 2c_{3x} + 2c_{4x} - 2c_{2x}, \\ Q_3 =& -2c_{1x} - 2c_{3x} + 2c_{4x} + 2c_{2x}, \\ G_1 =& 2c_{2y} - 2c_{4y} + 2c_{3y} - 2c_{1y}, \\ G_2 =& -2c_{2y} + 2c_{4y} + 2c_{3y} - 2c_{1y}, \\ G_3 =& 2c_{2y} + 2c_{4y} - 2c_{3y} - 2c_{1y}, \\ T_1 =& -2c_{1z} + 2c_{3z} - 2c_{4z} + 2c_{2z}, \\ T_2 =& -2c_{1z} + 2c_{3z} + 2c_{4z} - 2c_{2z}, \\ T_3 =& -2c_{1z} - 2c_{3z} + 2c_{4z} + 2c_{2z}, \\ R_1 =& c_{1y}^2 + c_{1x}^2 - c_{3y}^2 - c_{2x}^2 - c_{3x}^2 \\ & + c_{1z}^2 + c_{4x}^2 - c_{2z}^2 - c_{2y}^2 + c_{4y}^2 + c_{4z}^2 - c_{3z}^2, \\ R_2 =& c_{1y}^2 + c_{1x}^2 - c_{3y}^2 + c_{2x}^2 - c_{3x}^2 \\ & + c_{1z}^2 - c_{4x}^2 + c_{2z}^2 + c_{2y}^2 - c_{4y}^2 - c_{4z}^2 - c_{3z}^2, \\ R_3 =& c_{1y}^2 + c_{1x}^2 + c_{3y}^2 - c_{2x}^2 + c_{3x}^2 \\ & + c_{1z}^2 - c_{4x}^2 - c_{2z}^2 - c_{2y}^2 - c_{4y}^2 - c_{4z}^2 + c_{3z}^2. \end{aligned} \tag{27}$$

Solving the system given by Eq. (26) using Cramer's rule, the coordinates x, y, z are obtained as a function of θ_z.

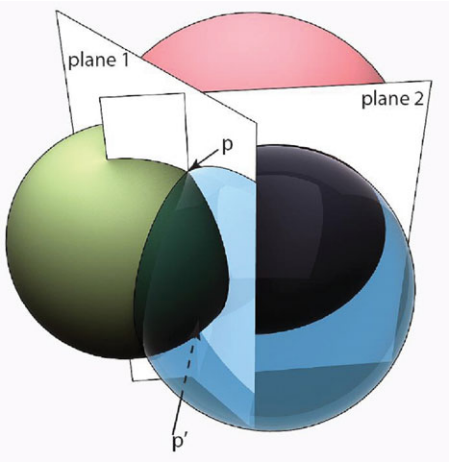


Fig. 4. Intersection of three spheres.

Now substituting in one of the sphere's equations, for example Eq. (18), and making use of the trigonometric identity,

$$s = \tan\frac{\theta_z}{2}, \tag{28}$$

the univariate polynomial of order 8 is obtained,

$$\begin{aligned} &l_1 s^8 + l_2 s^7 + l_3 s^6 + l_4 s^5 + l_5 s^4 + l_6 s^3 + l_7 s^2 + l_8 s \\ &\quad + l_9 = 0, \end{aligned} \tag{29}$$

where each l_i only depends on the geometrical properties of the mechanism and the input values q_i. Now the value of the platform angle θ_z is found numerically. For $\theta_z \neq 0$, the solutions are obtained back substituting the values of θ_z into the solutions of system (see Eq. (26)).

For $\theta_z = 0$, the system (see Eq. (26)) becomes linearly dependent, so the solution cannot be achieved by this method. In this case the intersection of three of the four spheres is analyzed. Knowing the position of the limbs is admitted that the intersection of three and four spheres is always possible. Thus, subtracting Eq. (19) from Eq. (18), and Eq. (20) from Eq. (18), two planes are obtained. These planes result from the intersection of the sphere C_1 with C_2 and C_2 with C_3, namely,

$$\text{plane 1} : m_1 x + m_2 y + m_3 z + m_4 = 0, \tag{30}$$

$$\text{plane 2} : m_5 x + m_6 y + m_7 z + m_8 = 0, \tag{31}$$

where m_i depends on the geometrical properties and the input values of the mechanism. The parametric equations of the common line to both planes are obtained as

$$\begin{aligned} x &= s_1 + s_2\lambda, \\ y &= s_3 + s_4\lambda, \\ z &= \lambda, \end{aligned} \tag{32}$$

where λ is the parameter and s_i depends on the geometrical properties and input values of the mechanism. Now, as can be seen in Fig. 4, intersecting the line with one of the spheres,

https://doi.org/10.1017/S0263574711000063 Published online by Cambridge University Press

the coordinates corresponding to the two solutions P and P', are obtained. Finally, the coordinates of these points are substituted into the equation of the fourth-sphere Eq. (21) to verify whether they are a solution of the direct position problem.

3.2. Inverse position problem

The inverse position problem aims to obtain the input values q_i for a given output value of the MP (x, y, z, θ_z). Using Eqs. (18)–(21) and considering x, y, z and θ_z to be known, making

$$\begin{aligned} X_i &= k\,(-d\cos\theta_z - c + h),\\ Y_i &= k\,(-d\sin\theta_z + a), \qquad (33)\\ i &= 1, 3, \end{aligned}$$

$$\begin{aligned} X_i &= k\,(d\sin\theta_z + a),\\ Y_i &= k\,(-d\cos\theta_z - c + h), \qquad (34)\\ i &= 2, 4, \end{aligned}$$

with k defined in Eq. (12). Now substituting each Eq. (18) into Eq. (21) and simplifying the result, the following expression is obtained:

$$T_i - 2bz\sin q_i - 2kb\,(\delta_i - \Delta_i)\cos q_i = 0, \quad i = 1, \ldots, 4, \tag{35}$$

where

$$\delta_i = \begin{cases} x, & i = 1, 3,\\ y, & i = 2, 4, \end{cases} \qquad \Delta_i = \begin{cases} X_i, & i = 1, 3,\\ Y_i, & i = 2, 4, \end{cases}$$

and

$$T_i = [(x - X_i)^2 + (y - Y_i)^2 + z^2 + b^2 - r^2],$$

where the variable sought is the input value q_i. Making use of the trigonometric identity ($t_i = \tan\frac{q_i}{2}$), a polynomial of second order in t_i is obtained:

$$t_i^2\,[T_i + 2b\,(\delta_i - \Delta_i)] - t_i\,(4bz) + [T_i - 2b\,(\delta_i - \Delta_i)] = 0. \tag{36}$$

Equation (36) gives the input values as a function of the MP position. In order to ensure the solution validity, both polynomial roots are obtained:

$$t_i = \frac{4bz \pm \sqrt{(4bz)^2 - 4\left[T_i^2 - 4b^2\,(\delta_i - \Delta_i)^2\right]}}{2\,[T_i + 2kb\,(\delta_i - \Delta_i)]}. \tag{37}$$

Back substitution of t_i produces two values of q_i for each Eq. (37), values that correspond to the ambiguity in the arc tangent function. In order to choose the correct value, we have to verify the result with each Eqs. (18)–(21) to check the validity of the solution.

From Eq. (37) one can see that the total number of solutions is 2^4. These solutions are the working modes of the manipulator. This means that for an output solution of the moving platform, each input rotary actuator q_i can have two different solutions. In order to avoid the manipulator changing between the working modes during tasks, input limits are required. In the case of this manipulator, these are $q_i \in [-90^\circ;\ 70^\circ]$. For reasons associated with construction, the upper limit has been set to 70° but, theoretically, only one solution can be found for $q_i \in [-90^\circ;\ 90^\circ]$. Furthermore, for better control of the limits the passive parameters can be used.

3.3. Workspace

In Eq. (37), the condition of having a positive value under the square root, as required for real solutions, provides one condition for the workspace:

$$(4bz)^2 - 4\left[T_i^2 - 4b^2\,(\delta_i - \Delta_i)^2\right] \geq 0 \quad i = 1, \ldots, 4. \tag{38}$$

Upon simplifications and back substitutions, this gives

$$\begin{aligned} &[(x - X_i)^2 + (y - Y_i)^2 + z^2 + b^2 - r^2]^2\\ &\quad \geq 4b^2[(\delta_i - \Delta_i)^2 + z^2], \quad i = 1, \ldots, 4. \end{aligned} \tag{39}$$

Equation (39) is the Cartesian equation of the four tori with center at point $(X_i, Y_i, 0)$, axis parallel to $\boldsymbol{j}$ for $i = 1, 3$ and parallel to $\boldsymbol{i}$ for $i = 2, 4$, radius of the tube r, and b is the distance from the center of the tube to the center of each torus, as shown in Fig. 5 for the first leg. As it can be seen, the planes P_1 and P_2 represent the superior and inferior limits of the input rotary values q_i. So, the rotation of the limb A_iB_i, represented by the length b, is restricted between -70° and 90°.

Finally, the workspace of the manipulator is geometrically obtained as the intersection of the four tori. In Fig. 6 the constant orientation workspace is shown for two different sets of design parameters of the manipulator and restricted to input values between -70° to $+90^\circ$. In line with this, Fig. 6(b) shows a workspace volume that is only 64% of the one shown in Fig. 6(a).

As can be observed, the design parameters h, a, b, r, c, and d and the orientation angle θ_z have a major influence on the size and the shape of the workspace. Hence, for workspace maximization these parameters have to be taken into account together with the limits of the rotary inputs.

4. Jacobian Analysis

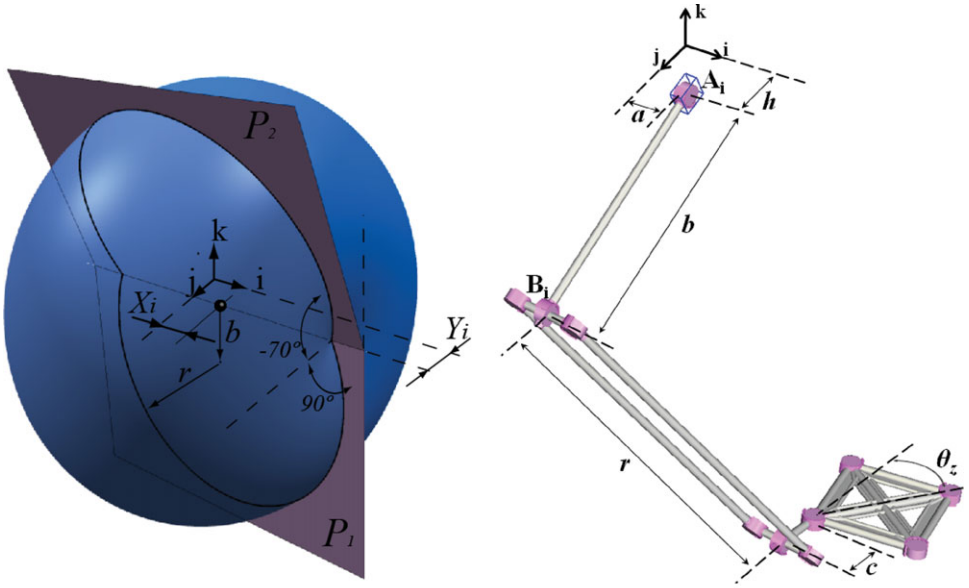
Differentiating the position equations with respect to time, Eq. (9) gives

$$\begin{aligned} &\dot{\boldsymbol{p}} = \dot{\boldsymbol{q}}_i \times (\boldsymbol{b}_i - \boldsymbol{a}_i) + \boldsymbol{\omega}_i \times (\boldsymbol{a}_i - \boldsymbol{b}_i) + \boldsymbol{\omega}_p \times (\boldsymbol{p} - \boldsymbol{d}_i),\\ &i = 1, \ldots, 4, \end{aligned} \tag{40}$$

where $\dot{\boldsymbol{p}}$ is the velocity of the operating point of the end-effector, $\dot{\boldsymbol{q}}_i$ is the input joint rates vector, $\boldsymbol{\omega}_i$ is the angular velocity of the passive parallelogram, and $\boldsymbol{\omega}_p$ is the angular velocity of the end-effector. Upon dot multiplication by

$$\mathbf{r}_i = \frac{1}{r}(\mathbf{c}_i - \mathbf{b}_i), \quad i = 1, \ldots, 4, \tag{41}$$

https://doi.org/10.1017/S0263574711000063 Published online by Cambridge University Press



(a) Torus (b) First limb of the manipulator

Fig. 5. Torus representation for the first leg with limits in the actuators.

we cancel passive joint rates to yield

$$\boldsymbol{r}_i \cdot \dot{\boldsymbol{p}} = \dot{\boldsymbol{q}}_i \cdot [(\boldsymbol{b}_i - \boldsymbol{a}_i) \times \boldsymbol{r}_i] + \boldsymbol{\omega}_p \cdot [(\boldsymbol{p} - \boldsymbol{d}_i) \times \boldsymbol{r}_i], \quad i = 1, \ldots, 4. \tag{42}$$

Bearing in mind that

$$\boldsymbol{\omega}_p = \dot{\theta}_z \boldsymbol{k} \tag{43}$$

and rearranging terms, we obtain

$$\dot{\theta}_z \mathbf{k} \cdot [(\mathbf{p} - \mathbf{d}_i) \times \mathbf{r}_i] + \mathbf{r}_i \cdot \dot{\mathbf{p}} = \dot{\mathbf{q}}_i \cdot [(\mathbf{b}_i - \mathbf{a}_i) \times \mathbf{r}_i]. \tag{44}$$

If we use

$$\begin{aligned} \dot{\mathbf{q}}_1 &= -\dot{q}_1 \mathbf{j}, \\ \dot{\mathbf{q}}_2 &= \dot{q}_2 \mathbf{i}, \\ \dot{\mathbf{q}}_3 &= \dot{q}_3 \mathbf{j}, \\ \dot{\mathbf{q}}_4 &= -\dot{q}_4 \mathbf{i}, \end{aligned} \tag{45}$$

and arranging in matrix form this gives

$$\mathbf{J}_v \mathbf{t} = \mathbf{J}_q \dot{\mathbf{q}}, \tag{46}$$

where

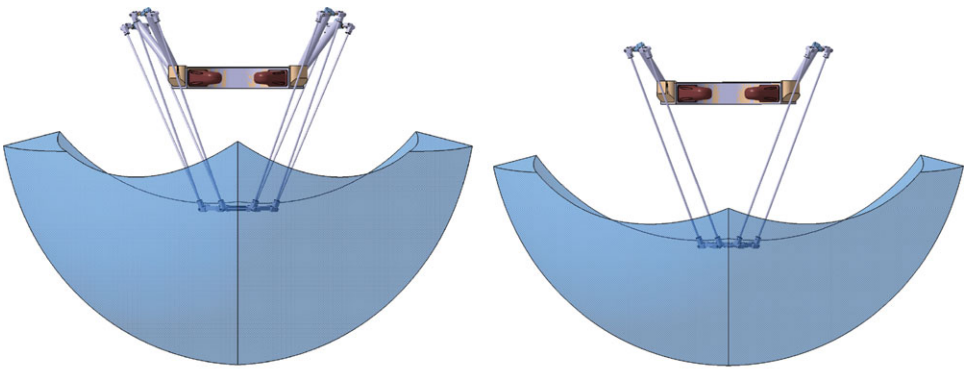
$$\mathbf{t} = \left[\dot{\theta}_z \ \dot{\mathbf{p}}^T\right]^T$$

is the four-dimensional MP twist, the actuated-joint-rate vector is defined as

$$\dot{\mathbf{q}} = \left[\dot{q}_1 \ \dot{q}_2 \ \dot{q}_3 \ \dot{q}_4\right]^T, \tag{47}$$

and the Jacobian matrices $\mathbf{J}_v$ and $\mathbf{J}_q$ are

$$\mathbf{J}_v = \begin{bmatrix} \mathbf{s}_1^T \mathbf{k} & \mathbf{r}_1^T \\ \mathbf{s}_2^T \mathbf{k} & \mathbf{r}_2^T \\ \mathbf{s}_3^T \mathbf{k} & \mathbf{r}_3^T \\ \mathbf{s}_4^T \mathbf{k} & \mathbf{r}_4^T \end{bmatrix}, \quad \mathbf{J}_q = \begin{bmatrix} -\mathbf{n}_1^T \mathbf{j} & 0 & 0 & 0 \\ 0 & \mathbf{n}_2^T \mathbf{i} & 0 & 0 \\ 0 & 0 & \mathbf{n}_3^T \mathbf{j} & 0 \\ 0 & 0 & 0 & -\mathbf{n}_4^T \mathbf{i} \end{bmatrix}, \tag{48}$$



(a) $b = 0.4$, $c = 0.1$, $d = 0.07$ (b) $b = 0.3$, $c = 0.05$, $d = 0.068$

Fig. 6. Constant orientation workspace for the symmetric Schönflies-motion generators with $h = 0.275$, $a = 0.125$, $r = 1$ $[m]$.

https://doi.org/10.1017/S0263574711000063 Published online by Cambridge University Press

where

$$\begin{aligned}\mathbf{s}_i &= (\boldsymbol{d}_i - \boldsymbol{p}) \times \boldsymbol{r}_i \quad i = 1, \ldots, 4,\\ \mathbf{n}_i &= (\boldsymbol{b}_i - \boldsymbol{a}_i) \times \boldsymbol{r}_i \quad i = 1, \ldots, 4.\end{aligned} \tag{49}$$

The direct and inverse singularity locus can be obtained in the expressions of the determinant of $\mathbf{J}_v$ and $\mathbf{J}_q$, namely,

$$\begin{aligned}\|\mathbf{J}_v\| = {} & \mathbf{s}_1^T\mathbf{k}\,(\mathbf{r}_2 \cdot (\mathbf{r}_3 \times \mathbf{r}_4)) - \mathbf{s}_2^T\mathbf{k}\,(\mathbf{r}_1 \cdot (\mathbf{r}_3 \times \mathbf{r}_4))\\ & + \mathbf{s}_3^T\mathbf{k}\,(\mathbf{r}_1 \cdot (\mathbf{r}_2 \times \mathbf{r}_4)) - \mathbf{s}_4^T\mathbf{k}\,(\mathbf{r}_1 \cdot (\mathbf{r}_2 \times \mathbf{r}_3)),\end{aligned} \tag{50}$$

$$\left\|\mathbf{J}_q\right\| = \mathbf{n}_1^T\mathbf{j} \cdot \mathbf{n}_2^T\mathbf{i} \cdot \mathbf{n}_3^T\mathbf{j} \cdot \mathbf{n}_4^T\mathbf{i}. \tag{51}$$

4.1. Isotropy

The manipulator isotropy is often related to the dexterity and the determination of the most suitable postures within the workspace. The isotropic postures of the Jacobian matrices obtained in Eq. (46) must fulfil the relations given below

$$\mathbf{J}_v^T\mathbf{J}_v = \sigma^2\,\mathbf{I}, \tag{52}$$

$$\mathbf{J}_q^T\mathbf{J}_q = \tau^2\,\mathbf{I}, \tag{53}$$

where σ and τ denote the four identical singular values that each Jacobian matrix must have at the optimum postures.

In this case, because of the fact that the Jacobian matrix $\boldsymbol{J}_v$ contains mixed rotation and translation terms, a normalization must be obtained in order to homogenize $\boldsymbol{J}_v$. In order to cope with this problem, the *characteristic length* l_c[15] is proposed. Therefore, the left-hand side of the velocity equation (46) is rewritten as

$$\mathbf{J}_v\,\mathbf{t} = \begin{bmatrix}\mathbf{f}_\omega\ \mathbf{F}_p\end{bmatrix}\begin{bmatrix}\omega_z\\ \dot{\mathbf{p}}\end{bmatrix} = \begin{bmatrix}(1/l_c)\,\mathbf{f}_\omega\ \mathbf{F}_p\end{bmatrix}\begin{bmatrix}l_c\,\omega_z\\ \dot{\mathbf{p}}\end{bmatrix}, \tag{54}$$

where

$$\mathbf{F}_p = \begin{bmatrix}\mathbf{r}_1^T\\ \mathbf{r}_2^T\\ \mathbf{r}_3^T\\ \mathbf{r}_4^T\end{bmatrix}, \quad \mathbf{f}_\omega = \begin{bmatrix}\mathbf{s}_1^T\mathbf{k}\\ \mathbf{s}_2^T\mathbf{k}\\ \mathbf{s}_3^T\mathbf{k}\\ \mathbf{s}_4^T\mathbf{k}\end{bmatrix},$$

and the dimensional homogeneous Jacobian $\overline{\mathbf{J}}_v$ being obtained as

$$\overline{\mathbf{J}}_v = \begin{bmatrix}(1/l_c)\,\mathbf{f}_\omega\ \mathbf{F}_p\end{bmatrix}. \tag{55}$$

Now the isotropy condition can be expressed as

$$\overline{\mathbf{J}}_v^T\overline{\mathbf{J}}_v = \begin{bmatrix}(1/l_c^2)\,\mathbf{f}_\omega^T\mathbf{f}_\omega & (1/l_c)\,\mathbf{f}_\omega^T\mathbf{F}_p\\ (1/l_c)\,\mathbf{F}_p^T\mathbf{f}_\omega & \mathbf{F}_p^T\mathbf{F}_p\end{bmatrix} = \begin{bmatrix}\sigma^2 & \mathbf{0}^T\\ \mathbf{0} & \sigma^2\,\mathbf{I}_3\end{bmatrix}, \tag{56}$$

where $\mathbf{I}_3$ denotes the 3×3 identity matrix.

Hence, the characteristic length l_c is obtained from Eq. (56) as

$$l_c = \sqrt{3\,\frac{\mathbf{f}_\omega^T\mathbf{f}_\omega}{\operatorname{tr}\left(\mathbf{F}_p^T\mathbf{F}_p\right)}}. \tag{57}$$

Substituting Eq. (57) in Eq. (56), the isotropic postures of the manipulator are obtained in terms of the Cartesian coordinates of the moving platform:

$$\begin{aligned}&x_P = 0, \quad y_P = 0, \quad z_P = -\sqrt{b^2 - n^2} - \frac{\sqrt{3}\,r}{3}, \quad \theta_z = 0,\\ &\quad \text{for } n < 0,\\ &x_P = 0, \quad y_P = 0, \quad z_P = -\sqrt{b^2 - n^2} + \frac{\sqrt{3}\,r}{3}, \quad \theta_z = 0,\\ &\quad \text{for } n > 0,\\ &a = \frac{\sqrt{6}}{3}r, \quad a \le h, \quad b^2 - n^2 \ge 0,\\ &n = c + d\cos\theta_z - h,\end{aligned} \tag{58}$$

with the characteristic length being

$$l_c = d\sqrt{2},$$

and the common singular value

$$\sigma = \frac{2\sqrt{3}}{3}.$$

Positions where Jacobian matrix $\mathbf{J}_q$ is isotropic are now found directly, as $\mathbf{J}_q$ is dimensionally homogeneous. Indeed, if $x_P = y_P = 0$ and $\theta_z = 0$, then

$$\begin{aligned}\boldsymbol{J}_q^T\mathbf{J}_q &= \begin{bmatrix}m & 0 & 0 & 0\\ 0 & m & 0 & 0\\ 0 & 0 & m & 0\\ 0 & 0 & 0 & m\end{bmatrix},\\ m &= -\frac{b}{r}\,(n\sin q - z_P\cos q),\\ &\forall q = q_i,\ i = 1, \ldots, 4,\end{aligned} \tag{59}$$

where q is the rotary input of the manipulator, which, for these output coordinates x_P, y_P, is the same in all the limbs because of its symmetry. Thus, it can be seen that the isotropic postures of $\boldsymbol{J}_q$ are

$$x_P = y_P = 0, \quad \forall z_P, \quad \theta_z = 0,$$

and the common singular value is

$$\tau = \sqrt{m}, \tag{60}$$

with no conditions placed on the geometric parameters. Hence, the isotropic postures of the inverse Jacobian can be found for any geometric parameter configuration. In the case of the direct Jacobian, this is not possible because of the restrictions of a certain parameter of the manipulator as shown in Eq. (58).

In conclusion, the isotropic configurations are mainly influenced by the end-effector pose. The design parameters are also an important factor, knowing that these could

https://doi.org/10.1017/S0263574711000063 Published online by Cambridge University Press

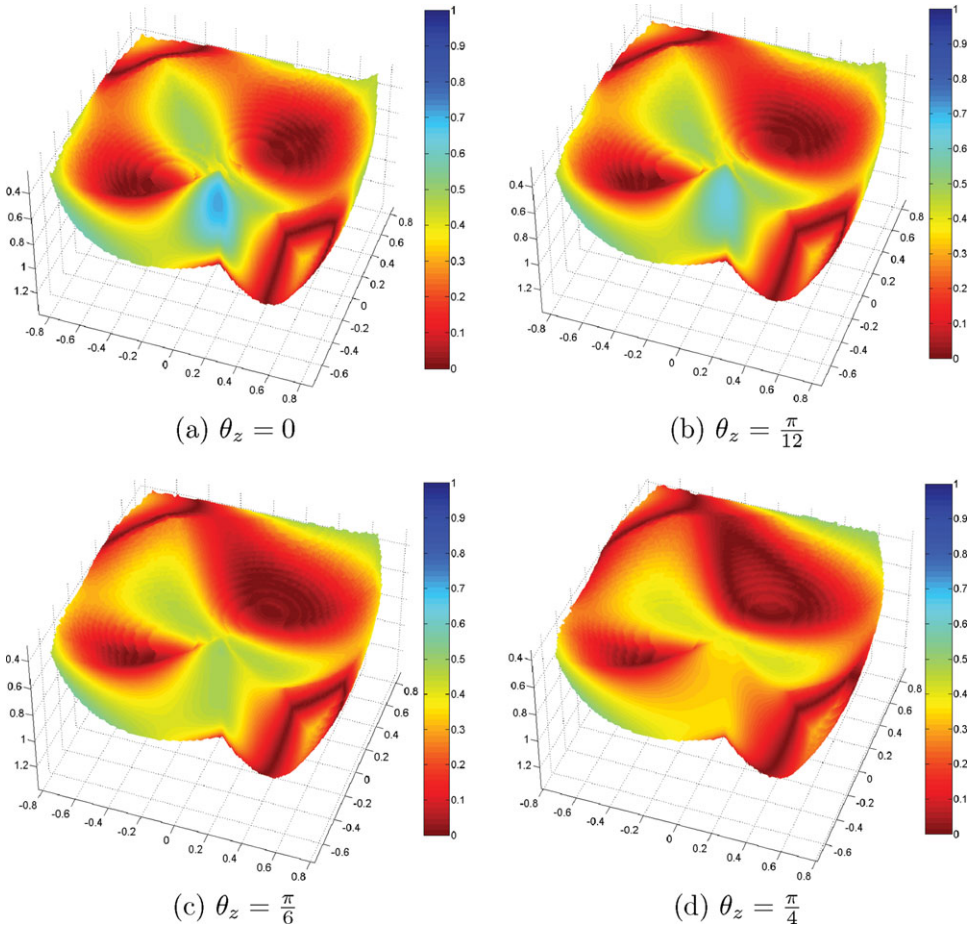


Fig. 7. Local dexterity map for $h = 0.275$, $a = 0.125$, $b = 0.4$, $r = 1$, $c = 0.102$, $d = 0.07$ $[m]$.

establish which set of design parameters is better for obtaining of the isotropic configurations. In this case, as it can be seen in Eq. (58), the isotropic poses within the workspace can be obtained for an unfeasible set of parameters, owing to the fact that the parameters c and d can be very large, affecting in this way not only the volume of the workspace but also the dynamic behavior.

4.2. *Dexterity*

In order to assess the dexterity, performance indices are frequently used, e.g., the condition number, the minimum singular value, or the manipulability.[16]

A performance index defined as the condition number κ_F, based on the weighted Frobenius norm,[17] was proposed in ref. [18], which is given by

$$\kappa_F\left(\bar{\mathbf{J}}_v\right) = \left\|\bar{\mathbf{J}}_v\right\|_F \left\|\bar{\mathbf{J}}_v^{-1}\right\|_F, \tag{61}$$

where $\bar{\mathbf{J}}_v$ is the Jacobian with a characteristic length introduced, and the weighted Frobenius norm is defined as

$$\left\|\bar{\mathbf{J}}_v\right\|_F = \sqrt{\frac{1}{4}\mathrm{tr}\left(\bar{\mathbf{J}}_v\,\bar{\mathbf{J}}_v^T\right)}. \tag{62}$$

In the following, the workspace volume has been numerically discretized using an equally spaced set of points and the local performance index has been evaluated at each of these points. As κ_F varies from unity to infinity, a scaled $1/\kappa_F$ has been used.

In Fig. 7, the index range varies from a singular posture (the nullity) to an isotropic one (the unity). The map has been sliced into by two planes, one at $x = y$ and the other at $x = -y$, in order to reveal points inside. As the workspace is symmetric, only a quarter of the volume has been cut away. One can observe that, for this set of design parameters, the local dexterity map varies with θ_z. In addition, as θ_z moves further from 0, the number of unsuitable positions $1/\kappa_F \approx 0$ increases and the number of suitable ones decreases. In fact, none of the latter reaches the isotropic posture ($1/\kappa_F = 1$) for this working mode as shown in Fig. 7. An angle of $\theta_z = 0$ should be taken into account in order to obtain a high dexterity within the workspace.

5. Amplification Mechanical Device

Fully symmetrical parallel manipulators with four limbs have an intrinsic limitation regarding angular positioning. The interference between links reduces the practical range of rotation, which is an important drawback for pick-and-place operations where $\pm\pi$ rotations are required. In order to meet this demand, we have proposed two alternatives of an angular multiplication device on the moving platform.

The first device is composed of a planetary gear, which is employed in the following way: the planetary gear carrier is attached to the moving platform of the parallel manipulator

https://doi.org/10.1017/S0263574711000063 Published online by Cambridge University Press

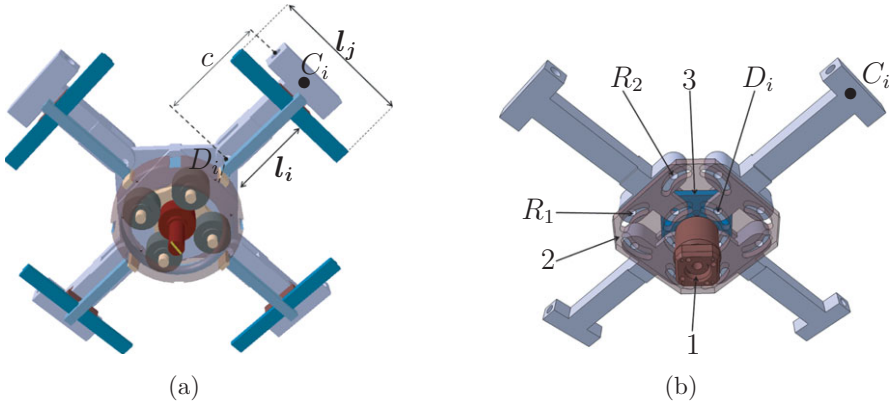


Fig. 8. Mechanical devices proposed for MP rotation multiplication.

that provides rotations of $\pm\frac{\pi}{4}$; the sun gear has its axle attached to the end-effector, which will provide the required $\pm\pi$; and the ring gear is kept in pure translation attached to a frame that translates with the moving platform. The multiplication factor will be equal to 4, sun and planet gears both having 18 teeth and the ring gear having 54. As shown in Fig. 8(a), the links $\overline{C_i D_i}$ translate. When rotation is produced, this translation is not always the same as that of the moving platform. As the sun gear axle is pin-joined to the MP center point, the ring gear follows the same translation pattern as the moving platform. This translation pattern includes two sliding bars, one in the direction of $\boldsymbol{l}_i$ at $\frac{\pi}{2}$ that connects to the second one in the direction of $\boldsymbol{l}_j$, which is fixed to each $\overline{C_i D_i}$ link through two prismatic pairs.

Another solution is shown in Fig. 8(b). In order to increase the rigidity of the mechanism, the two sliding bars have been eliminated and three circular sliders introduced at R_1, R_2, and D_i. In addition, a commercial multiplication device (MD, element 1 in Fig. 8(b)) with a multiplication factor of 6 has been introduced. Hence, the translational plate (FP, element 2 in Fig. 8(b)), together with the MD annulus, is directly connected between them. However, the MD sun gear input also connects with the moving platform (MP, element 3 in Fig. 8(b)). Thus, the MP, FP, and MD follow the same translation motion pattern. Moreover, when the moving platform rotates, only the multiplication device sun gear input follows the circular motion. In this way, neither the translational plate nor the multiplication device annulus will move and, thus, an amplification is possible at the sun gear output. At the same time, the circular sliders R_1, R_2, and D_i permit the relative movement of the link $C_i D_i$ (element 4 in Fig. 8b) with respect to the translational plate.

In Fig. 9, the prototype of the second solution is shown from the top and bottom views.

6. Conclusions

In this paper we have presented a symmetric parallel Schönflies-motion generator with a rigid moving platform and 4-dof. The direct position problem has been solved in a closed-form solution, and an alternative procedure, based on the intersection of three spheres, has been applied in the particular case of $\theta_z = 0$. The parallel manipulator described presents, in general, a wide operational workspace, which is design parameter and orientation-angle-dependent. Thus, the design needs optimization in order to maximize the workspace. The inverse and direct Jacobian has been also studied and the isotropic configuration has been found. The dexterity map shows the singularity locus dependency with the orientation angle variation. Moreover, it has been shown that the number of suitable postures is dependent on this variation. Hence, the dexterity optimization will be necessary in order to obtain a singularity-free workspace, if one exists. Finally, the design of two amplifier mechanical devices has been described so that the moving platform fulfils the rotation requirements of pick-and-place operations.

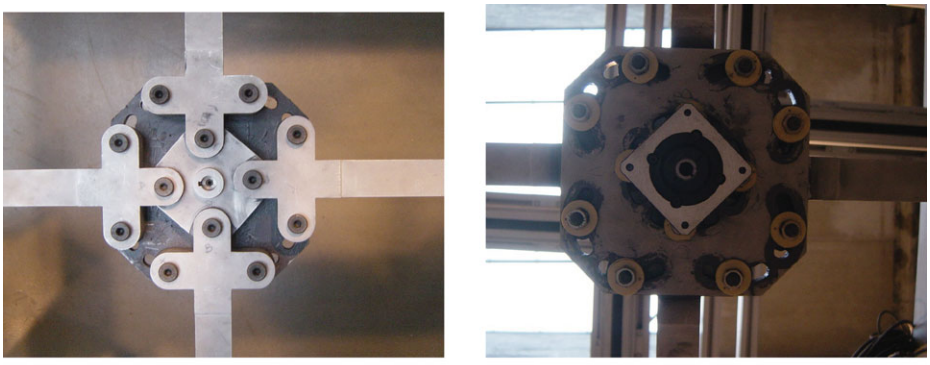


Fig. 9. Mechanical device prototype.

https://doi.org/10.1017/S0263574711000063 Published online by Cambridge University Press

In order to meet requirements as closely as possible, the manipulator needs a maximal operational workspace as well as good dexterity. Further work thus consists of calculating the workspace and dexterity kinematic functions and then using them in a multiobjective optimization design.

Acknowledgments

The authors wish to acknowledge the financial support received from the Spanish Government via the Ministerio de Educación y Ciencia (Project DPI2008-00159), the European Union (Project *FP7*-CIP-ICT-PSP-2009-3) and the Departamento de Educación, Universidades e Investigación of the Basque Government (Project IT445-10).

References

1. Z. Huang and Q. Li, "General methodology for type synthesis of symmetrical lower-mobility parallel manipulators and several novel manipulators," *Int. J. Robot. Res.* **21**(2), 131–145 (2002).
2. A. Fattah and G. Kasai, "Kinematics and dynamics of a parallel manipulator with a new architecture," *Robotica* **18**, 535–543 (2000).
3. R. Di Gregorio, "A new family of spherical parallel manipulators," *Robotica* **20**, 353–358 (2002).
4. L. Romdhane, Z. Affi and Z. M. Fayet, "Design and singularity analysis of a 3-translational-dof in-parallel manipulator," *ASME J. Mech. Des.* **124**, 419–426 (2002).
5. M. Ceccarelli, *Fundamentals of Mechanics of Robotic Manipulation* (Kluwer/Springer, Dordrecht, Netherlands, 2004) (ISBN 1-4020-1810-X).
6. J. Angeles, "The Degree of Freedom of Parallel Robots: A Group-Theoretic Approach," *Proceedings of the 2005 IEEE International Conference on Robotics and Automation*, Barcelona, Spain (April 18–22, 2005) pp. 1017–1024.
7. J. M. Hervé, "Analyse structurelle des mécanismes par groupe des déplacements," *Mech. Mach. Theory* **13**(4), 437–450 (1978).
8. X. Kong and C. Gosselin, "Type synthesis of 3T1R 4-DOF parallel manipulators based on Screw theory," *IEEE Trans. Robot. Autom.* **20**(2), 181–190 (2004).
9. J. Angeles, S. Caro, W. Khan and A. Morozov, "Kinetostatic design of an innovative Schönflies-motion generator," *Proc. I MECH E Part C J. Mech. Eng. Sci.* **220**(7), 935–943 (2006).
10. J.-F. Gauthier, J. Angeles, S. Nokleby and A. Morozov, "The kinetostatic conditioning of two-limb Schönflies motion generators," *ASME J. Mech. Robot.* **1**(1), 011010-1–011010-12 (2009).
11. P. L. Richard, C. M. Gosselin and X. Kong, "Kinematic analysis and prototyping of a partially decoupled 4-DOF 3T1R parallel manipulator," *ASME J. Mech. Des.* **129**(6), 611–616 (2007).
12. O. Company, F. Marquet and F. Pierrot, "A new high-speed 4-dof parallel robot synthesis and modelling issues," *IEEE Trans. Robot. Autom.* **19**(3), 411–420 (2003).
13. O. Salgado, O. Altuzarra, E. Amezua and A. Hernández, "A parallelogram-based parallel manipulator for Schönflies motion," *ASME J. Mech. Des.* **129**(12), 1243–1250 (2007).
14. L. W. Tsai, *Robot Analysis: The Mechanics of Serial and Parallel Manipulators* (Wiley & Sons, New York, 1999).
15. E. Schwartz, R. Manseur and K. Doty, "Noncomensurate systems in robotics," *Int. J. Robot. Autom.* **17**(2), 1–6 (2002).
16. T. Yoshikawa, "Manipulability of robot manipulators," *Int. J. Robot. Res.* **4**(2), 3–9, 1985.
17. G. H. Golub and C. F. Van Loan, *Matrix Computations*, 3rd ed. (The John Hopkins University Press, Baltimore, 1996).
18. W. A. Khan and J. Angeles, "The kinetostatic optimization of robotic manipulators: The inverse and the direct problems," *ASME J. Mech. Des.* **128**(1), 168–178 (2006).

https://doi.org/10.1017/S0263574711000063 Published online by Cambridge University Press